

Hyperbolic metamaterial resonator for broadband enhancement and photon collection of silicon carbide quantum emitters

F. A Inam^{1,2}, N. Ahmed¹, M. J. Steel³ and S. Castelletto⁴

¹Dept. of Physics, Aligarh Muslim University, Aligarh, U.P. 202002, India

²Dept. of Condensed Matter Physics and Material Science, Tata Institute of Fundamental Research, Mumbai 400005, India

³MQ Photonics Research Centre, Dept. of Physics and Astronomy, Macquarie University, Sydney, NSW 2109, Australia

⁴School of Engineering, RMIT University, Melbourne, Victoria 3001, Australia

Author e-mail address: faraz.inam.phy@amu.ac.in

Abstract:

We model the broadband enhancement of single-photon emission from color centres in silicon carbide (SiC) nanocrystals coupled to a planar hyperbolic metamaterial (HMM) resonator. The design is based on positioning the single photon emitters within the HMM resonator, made of a dielectric index-matched with SiC material, and using a nanoantenna for improved collection efficiency. We show that employing HMM resonators can result in a significant enhancement of the spontaneous emission of a single photon source and its collection efficiency, compared to previous designs.

Keywords: *Hyperbolic metamaterial resonator, Single-photon sources, Silicon Carbide emitters, Nanodiamond nitrogen vacancy centers, broadband enhancement.*

1. Introduction:

Solid-state quantum emitters operating at room temperature ^[1, 2] and their integration in photonic networks are central in the development of quantum information processing, including optical quantum computation and quantum cryptography. In recent years a variety of materials have emerged as an alternative platform to host color centres that could operate as room-temperature single photon sources (SPSs) ^[3, 4], and at the same time, as coherent spin quantum bits with optical read-out^[5, 6]. This category of quantum emitters includes diamond color centres^[7], zinc-oxide based (ZnO) color centres^[8], emitters in silicon-carbide (SiC)^[3], GaN^[9], and 2D materials such as boron nitride^[4]. While all these platforms are of great interest for future integrated on-chip quantum photonics at room temperature, as they all have their own set of interesting properties, only diamond and SiC have been proved to host SPSs and spin qubits with optical read-out at the same time^[5, 6]. In particular SiC can host bright SPSs in the visible^[10], that may be efficiently electrically driven using off-the-shelf fabrication methods^[11]. Further SiC possesses many color centres with high spin state^[3], that can be used as quantum bits with the longest coherence time in solids, due to the absence of spin-orbit coupling and nuclear spin bath decoupling^[12]. Additionally SiC is a CMOS

compatible material^[13] with a large variety of nanofabrication methods that includes laser micromachining/deposition and ablation^[14], making it ideally placed for device fabrication and on-chip integration of quantum systems^[15]. These quantum emitters' spectra range from the visible region to the near infrared (up to \sim 1100nm), the latter emitters being much dimmer^[6] and thus most in need of radiative spontaneous emission (SE) enhancement for their application in magnetic sensing^[16] and spin nanoscopy^[17].

As color centres are point objects emitting radiation as a point dipole with a slow decay rate (nanosecond scale), one of the main aims of the field is to increase their decay rate and direct their emission modes. The typical approach followed is to couple them with microcavities or nanocavities with high quality factors or small mode volume to increase the enhancement on a specific emission mode and couple them to waveguides to extract the photons^[2, 18]. For optical micro and nanocavities, achieving high Purcell enhancement dictates narrow linewidth, with high complexity in control of the position of quantum emitters in the cavity. Scalability and loss of emission due to the large phonon side band of most color centres in solids is a main hurdle. The other approach which has been targeted is to build a single photon antenna^[19] based on plasmonic resonators^[20]. Here the quality factor is low, thus enhancement can occur over the entire color center spectrum (100 nm), while high confinement can be achieved. One of the major disadvantages of plasmonic antennas is in relying on materials with plasmonic resonance which entails plasmonic losses^[21]. More recently a class of Hyperbolic Metamaterials (HMM)^[22], metal-dielectric multilayers, have been proposed to enhance the SE of SPSs due to their in-principle indefinitely large photonic density of states and have opened new avenues in their use for quantum optics applications, including SPSs. HMMs have an extremely anisotropic dielectric tensor, with dielectric properties in some directions and metallic properties in another direction, thus providing high emission directionality, indefinite increase of LDOS and thus of SE rate, with overall high quantum yield due to a larger ratio of radiated to dissipated power as compared to plasmonic antennas^[23]. All these properties are maintained over 100 to 200 nm spectral region. To increase the outcoupling of non-radiative plasmonic modes from the HMM, metallic diffraction gratings coupled with the HMM or nanopatterning of the HMMs have been introduced, eventually increasing the collection efficiency of integrated SPSs. The collection enhancement of quantum dots SE has been achieved when positioned within HMM resonators^[24], while for the nitrogen vacancy centre (NV) in nanodiamond, the nanodiamonds were positioned on top of the HMM resonators^[25]. This last case has achieved an

enhancement of SE of a factor of 3, relative to the emission on a cover glass. Further by introducing a metalloid as metamaterial rather than gold, such as TiN, with lower dissipative losses, a SE enhancement close to 10 for a perpendicular dipole was predicted (5.5 for the average dipole orientation) with an experimental average enhancement of a factor of 4^[26].

In this work we study and design a HMM resonator based on only five alternating layers of gold and ZnS (previously 16 layers were used^[26]) for non-resonant broad-band enhancement of SE of SiC emitters^[27]. The emitter is positioned in the centre of the resonator rather than on the top. In this case the position of the quantum emitter is not critically dependent on the horizontal location and an antenna is used to enhance the SPS's collection efficiency. It is thus the first broadband design specifically targeting emitters, such as the carbon antisite vacancy pair^[10] and other visible SiC surface quantum emitters^[11], the silicon vacancy in SiC^[6], and it could be as well applied to NV centres in diamond. The choice of ZnS as dielectric is based on its facile deposition methods with its wide use in thin-film growth^[28] and most importantly its refractive index (2.4) being similar to SiC (2.5) and diamond (2.4). Emitters in high index dielectric materials like diamond/SiC generally suffer from low emission rates due to poor index matching at the diamond-air interface^[29]. Various methods have been explored to efficiently out-couple the emission from these emitters by placing them in an environment of higher refractive index materials^[30]. A ZnS resonator with its index matched with both diamond and SiC will be an ideal candidate for out-coupling of emission from these host centres and will result in enhanced emission rates. A ZnS resonator will be useful in coupling of nanocrystals of SiC containing the red or near infrared emitters^[6] or nanodiamonds containing NV centres. The use of SiC thin layers achieved by pulsed laser deposition^[31] as a dielectric in the HMM resonators, being the ultimate goal to apply this design to emitters directly embedded in the dielectric constituent^[32] of the HMM resonator. This design provides a factor of about 150 enhancement at both visible (680 nm, corresponding to the peak of diamond NV centre emission) and near infrared emission (900 nm, corresponding to the emission of SiC nanoparticles) relative to emission on a coverglass surface (the standard and most common measurement scheme) along with a Purcell factor enhancement ($\Gamma_{HMM}/\Gamma_{vacuum}$) of about 300 for perpendicular dipole orientation. By using a simple cubical patch antenna on the HMM resonator an improvement in the net collection power from about 0.1% to 15% can be achieved. This design is therefore universal to almost all solid-state single photon sources and results in broadband, ultrafast light emission and collection of the emitter's spontaneous emission.

The outline of the paper is as follows. In section 2 we discuss the theory of dipole emission in an HMM resonator as the one we are modeling. In section 3, the results section, we discuss the design of our HMM structure and study the Purcell enhancement associated with perpendicular and parallel dipole orientations, discussing the origin of the high enhancement relative to the perpendicular orientation. We then discuss how to extract light out of the structure by employing a simple Au-based cylindrical nano-antenna and cubical nanoscale patch antenna. In section 4, the method section, we discuss the details of our calculation scheme. Finally, in section 5, we conclude and provide an outlook on this HMM resonator fabrication.

2. Theory:

The spontaneous emission rate Γ of a quantum emitter can be accelerated by tuning the electromagnetic mode environment in its vicinity through a factor known as the local density of optical states (LDOS), $\rho(\mathbf{r}, \omega)$. The LDOS in terms of the Green function is defined as^[19, 33]

$$\rho(\mathbf{r}, \omega) = (6\omega/\pi c^2) [\hat{\mathbf{d}}^T \cdot \text{Im } G(\omega; \mathbf{r}, \mathbf{r}) \cdot \hat{\mathbf{d}}] \quad (1)$$

for the emitter source located at \mathbf{r} and oriented along the unit vector $\hat{\mathbf{d}}$. Here ω is the transition frequency and G is the dyadic Green function signifying the interaction of the radiated electric field with the emitter at the source point.

The enhancement of the spontaneous emission by an environment with high LDOS is known as the Purcell effect, which is quantified in terms of the Purcell factor, i.e. the spontaneous emission decay rate in such an environment compared to that in vacuum. A resonant structure provides an emitter with enhanced LDOS for its emitted photon to couple to when its emission frequency matches with the frequency of the optical modes supported by the structure. In plasmonics, large electric field in the vicinity of the metallic nano-structures significantly enhances the LDOS over the broad scattering spectrum of the metallic nano-structures. Plasmonic structures however provide enhanced LDOS mostly in the visible region of the spectrum as the resonant plasma frequency of the metals lies in this range. A hyperbolic meta-material (HMM) comprises of sub-wavelength scale periodic metal-dielectric layers in a specific direction^[22]. This provides anisotropy in the dispersion profile resulting in anisotropy in the LDOS for different transition dipole orientations as well as divergence of the LDOS^[22]. In HMMs the modes have higher momentum than conventional surface plasmon polaritons, even out of resonance.

From the layers' permittivity and the exact fill fraction of metal in the structure the components of the effective anisotropic permittivity can be calculated using effective medium theory^[34]. The average index for the multilayered HMM can be calculated using the relation^[22]:

$$\epsilon_{\perp} = \frac{\epsilon_m d_m + \epsilon_d d_d}{d_m + d_d}, \quad \frac{1}{\epsilon_{\parallel}} = \frac{d_m / \epsilon_m + d_d / \epsilon_d}{d_m + d_d} \quad (2)$$

where $\epsilon_{\perp}, \epsilon_{\parallel}$ are the dielectric components in perpendicular and parallel directions respectively and d_m, d_d are the thickness of metal and dielectric layers respectively. In HMM the effective permittivity components ϵ_{\parallel} parallel and perpendicular ϵ_{\perp} to the interface have opposite signs ($\epsilon_{\perp} \cdot \epsilon_{\parallel} < 0$), which lends a hyperboloid shape to the iso-frequency surface (IFC), according to the dispersion relation equation $\frac{k^2_{\parallel}}{\epsilon_{\parallel}} + \frac{k^2_{\perp}}{\epsilon_{\perp}} = \frac{\omega^2}{c^2}$. In the case of our ZnS/Au HMM structure (described in section 3 of the draft), the above hyperbolicity condition is well displayed within our studied frequency range of 650 nm to 1000 nm (Fig. 1).

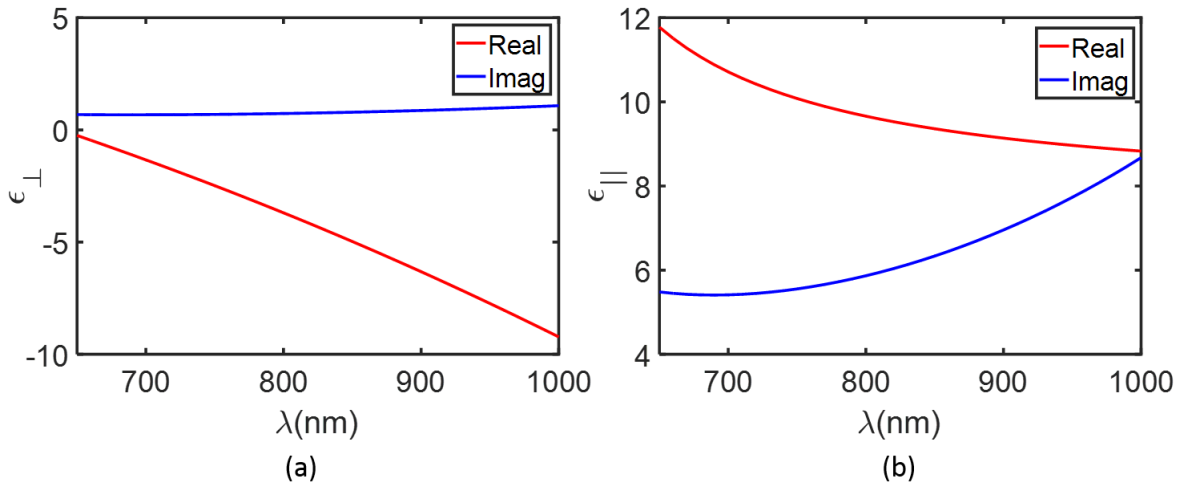


Figure 1. The effective permittivity (a) ϵ_{\perp} and (b) ϵ_{\parallel} of our ZnS/Au HMM structure as a function of wavelength.

There are two types of resonant modes arising in a HMM structure. The first is that of the plasmonic modes resulting from the alternate sub-wavelength metal layers. The second type are the structure modes as the HMM structure acts as a nanoscale lossy cavity. An interplay of these two type of modes results in the broadband enhancement of the LDOS seen by the transition dipole when placed inside the HMM^[35].

3. Results:

We carried out calculations using the Radio Frequency (RF) module of the COMSOL Multiphysics suite. To test the validity of our calculations we compared our results with the analytical results of a dipole emission near a metal film (Drexhage experiment)^[36]. Figure 2 shows the good agreement of our calculations with the analytical results. In this model we have a dipole emitter positioned in air and 10 nm away from the gold (Au) surface (Fig. 2a).

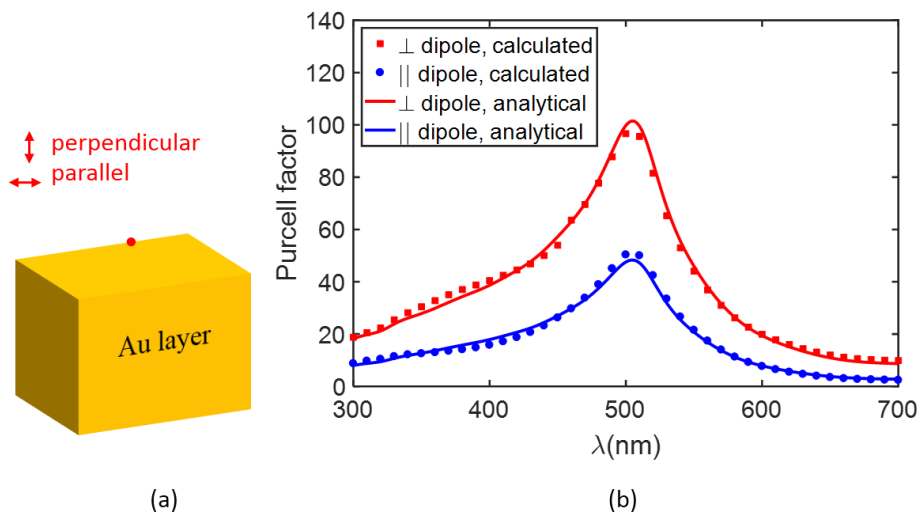


Figure 2. (a) Schematic of a dipole emitter placed on top of the gold (Au) surface. The separation between the dipole and Au surface is considered as 10 nm. (b) Calculated and analytical Purcell factor (Γ/Γ_{vacuum}) for the above considered case of dipole emission above the Au surface.

For this HMM calculation, we have considered quantum emitters based on silicon-carbide (SiC) nano-particles.

3.1. Purcell factor/emission rate calculations:

3.1.1 Designing of our broadband HMM structure: Tuning the Purcell enhancement by changing the index of the dielectric layers:

We start the design of HMM structure by encapsulating the nano-spheres of silicon-carbide of diameter 40 nm inside a Poly Vinyl Alcohol (PVA) matrix of thickness 50 nm. The PVA layer is encapsulated on both sides by gold (Au) metal layers of 30 nm thickness. To provide the hyperbolicity to this structure we place a low index dielectric layer of PVA of the same thickness 30 nm above and below the Au layers. This arrangement gives a simple five-layer structure of an HMM. The quantum emitter is placed at the centre of the SiC sphere. The HMM structure is placed on a glass substrate. From this simple low-index PVA/Au HMM, we build our HMM structure by sequentially replacing the PVA layer with the high indexed

layer of ZnS (Fig. 3). The ZnS layer has its index matched with the SiC nanoparticle and acts as an effective resonator for enhanced emission from SiC centres.

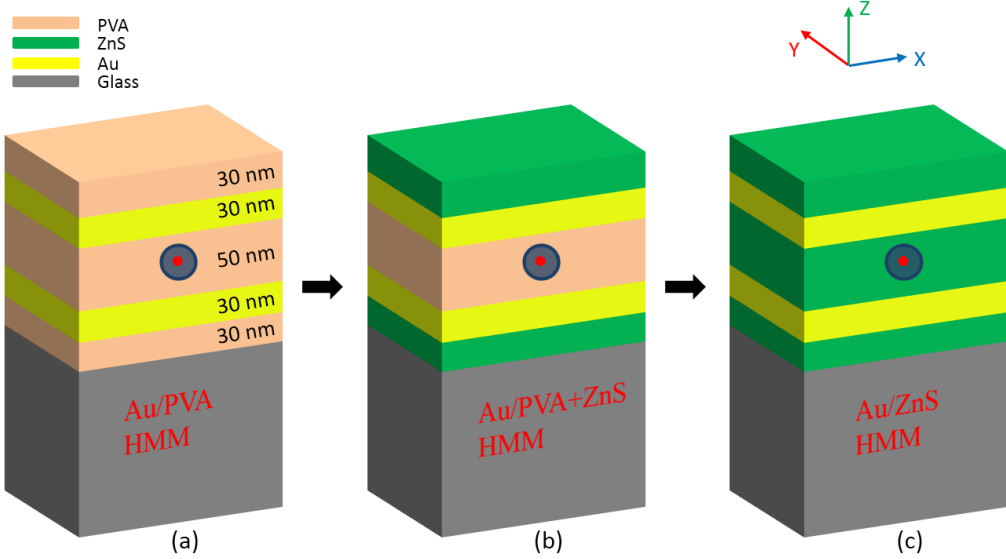


Figure 3. Schematic images showing the design for Au/ZnS HMM starting from a simple Au/PVA counterpart. (a) Au/PVA HMM, (b) Au/PVA+ZnS HMM and (c) Au/ZnS HMM.

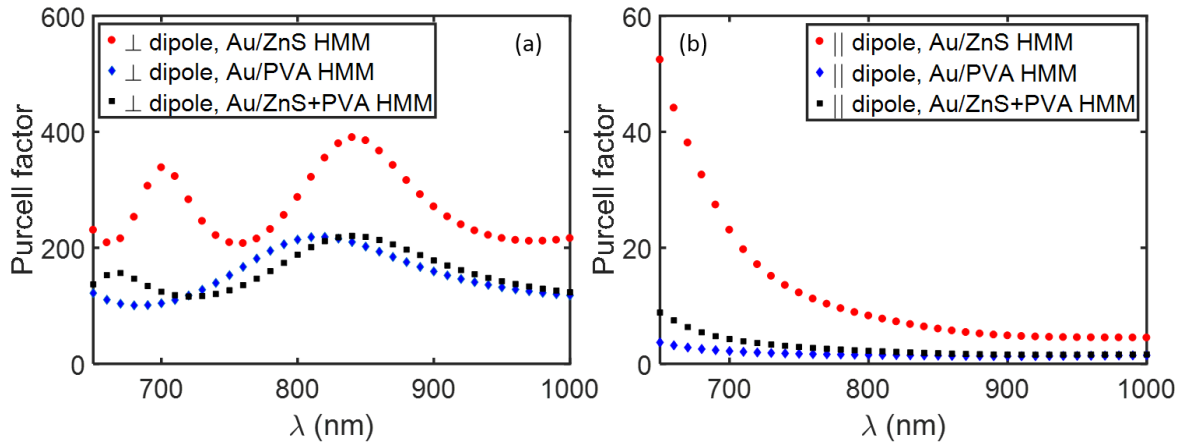


Figure 4. Purcell factor ($\Gamma_{HMM} / \Gamma_{vacuum}$) for dipole emission in the above three HMM structures corresponding to (a) perpendicular dipole orientation relative to the Au layers and (b) parallel dipole orientation relative to the Au layer.

Figure 4 displays how the Purcell factor ($\Gamma_{HMM} / \Gamma_{vacuum}$) for dipole emission in the HMM structure is significantly enhanced by the use of index-matched ZnS layers. On replacing the PVA layer ($n = 1.47$ at $\lambda = 900$ nm) with the high index ZnS layer ($n = 2.30$ at $\lambda = 900$ nm) the enhancement in the Purcell factor/emission rate significantly increases. More prominent resonance peaks emerge in the emission spectrum.

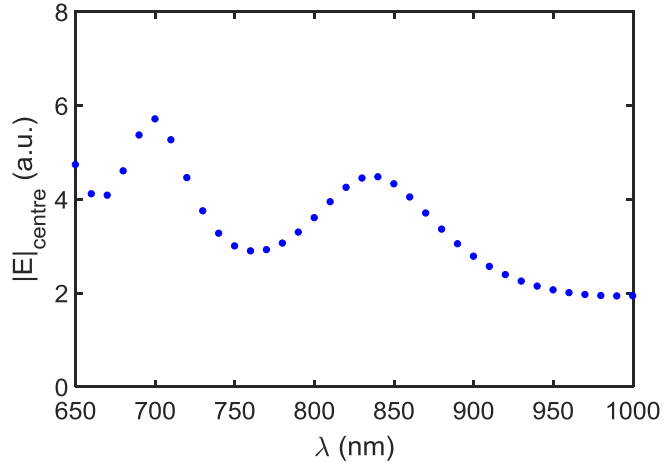


Figure 5. Electric field norm at the centre of the Au/ZnS HMM structure (at the dipole position) for perpendicular dipole excitation.

Figure 5 shows the electric field norm at the centre of the Au/ZnS HMM structure (at the dipole position) for perpendicular dipole excitation. Similar successive peaks in the electric field profile are seen as in the Purcell factor enhancement curve (Fig. 4). These successive peaks results from the lossy Fabry-Perot structure modes^[36]. The broadband response is restricted to the case of dipole emission perpendicular to the Au interface. Perpendicular dipole emission experiences reflections at the top and bottom HMM layers. This results in the excitation of lossy Fabry-Perot modes in the HMM structure. The mixing of the plasmonic modes with these structure modes results in the overall broadband response from the structure.

Here we have chosen a thickness for the metal/dielectric layers for which the HMM structure could be easily fabricated. Thinner metal/dielectric layers would have resulted in higher Purcell enhancement but then we would have required multiple layers and those would be more difficult to control experimentally. The resonance of these structure modes can further be optimized and tuned across the infrared spectrum by controlling the metal and dielectric layer thicknesses.

For the parallel dipole emission, the reflections at the top and bottom HMM layers are minimal due to the continuity of the field across the interface boundaries. The Purcell/emission enhancement is therefore restricted to only the plasmonic resonance in the visible spectrum without any structure modes arising in the infrared region (Fig. 5 (b)).

For the rest of this paper, we restrict our study to the case of perpendicular dipole emission in Au/ZnS HMM which shows enhanced broadband response with successive resonance peaks in the infrared spectrum where the emission from SiC as well as diamond centres lies.

3.1.2. The enhancement is not specific to the dipole's central position:

To test the sensitivity in the Purcell/emission enhancement with the variations in the dipole positions within the SiC nanoparticles we varied the dipole position along the z (vertical) and the x (horizontal) directions. The x and y directions which are both parallel to the metal-dielectric interface are symmetric to each other. The HMM structure is considered to be continuous along the x , y (horizontal) directions and we have modelled these by using scattering boundary conditions along these directions. Figure 6 shows the variation in the Purcell factor with dipole displacement along the three orthogonal coordinate axes for the case of dipole emission at 900 nm, corresponding to vacancy-Si, V_{Si} in SiC. Along the z -direction, as the dipole separation from the centre increases the dipole gets closer to the metal layers leading to significantly enhanced HMM structure modes coupled to the plasmonic resonance. Along the x and y directions, the dipole experiences the same electromagnetic environment due to the top and bottom HMM layer. Slight changes in the Purcell factor arise due to small variations in the dipole emission rates corresponding to the varying dipole separation from the SiC sphere surface for the vacuum case. Our result therefore shows that the enhancement is not specific to the dipole central location and the same order of enhancement exists for all dipole positions within the middle ZnS layer.

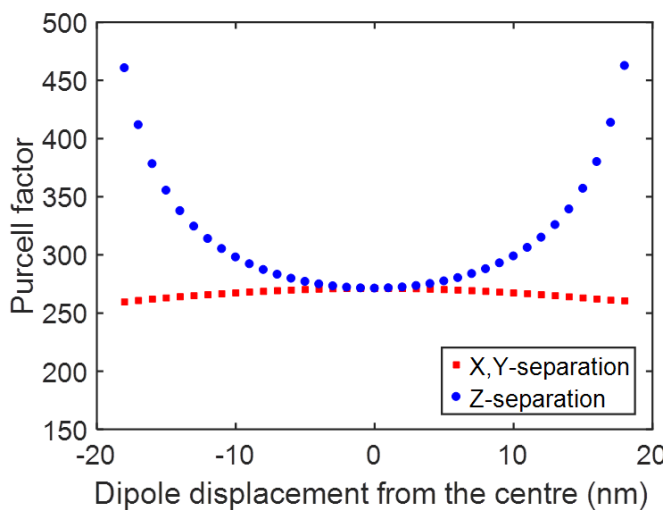


Figure 6. Variation of Purcell factor SiC based dipole emitter encapsulated in the multilayered Au/ZnS HMM structure with its displacement along the coordinate axes directions. The emission wavelength considered here is 900 nm corresponding to vacancy-Si, V_{Si} in SiC.

3.2. Collection efficiency calculations:

We have achieved broadband enhancement from visible to infra-red frequencies using a multilayered higher index dielectric HMM structure. We will now focus on how to capture the maximum light out of these structures. For this we calculate the collection efficiency of our HMM structure. We scaled our calculations relative to the collection efficiency for the case of SiC spheres on a coverglass which is the common measurement scheme. A lens surface with a numerical aperture (NA) 0.6 was modelled to collect the light from the top surface of the HMM as well as the coverslip.

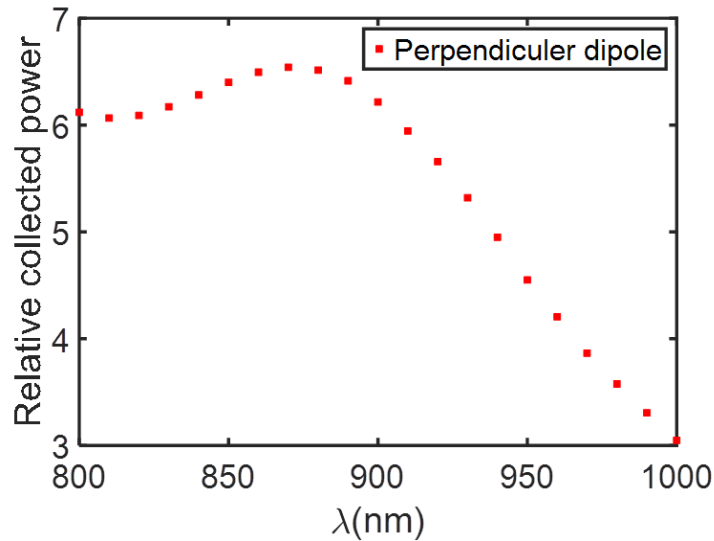


Figure 7. Relative collected power for dipole emission in our HMM structure considering collection lens numerical aperture to be 0.6. The collected power is relative to the collected power from the same emitter when the SiC particles are placed on a glass surface.

From figure 7 it is clear that the periodic layered grating-like structure of the HMM leads to significant scattering of the emitter's light. The relative enhancement in the collected power is therefore much smaller compared to the Purcell enhancement in the emission rates due to the HMM structure.

3.2.1. Design of a single photon antenna to enhance the light collection:

To collect light from the top of HMM structures, complex periodic-gratings are commonly used^[24, 30]. Here we use a simple antenna structure consisting of a single metal cylinder on top of the HMM structure. Traditionally for radio frequencies, antenna parameters are prescribed only in terms of external wavelength. However, at optical frequencies electrons in the metal offer substantial inertia and do not respond instantaneously to the driving fields. Metal electrons therefore have to be treated as a strong coupled plasma at optical frequencies. This

leads to a reduced effective wavelength within the antenna^[37]. To optimize the antenna parameters for maximum collection efficiency we measured the collected power from the structure by varying the antenna height at dipole emission wavelength equal to 900 nm. The diameter of the cylinder is kept fixed at 30 nm. The calculated optimum antenna height for 900 nm emission wavelength is around 105 nm (Figure 8 (b)).

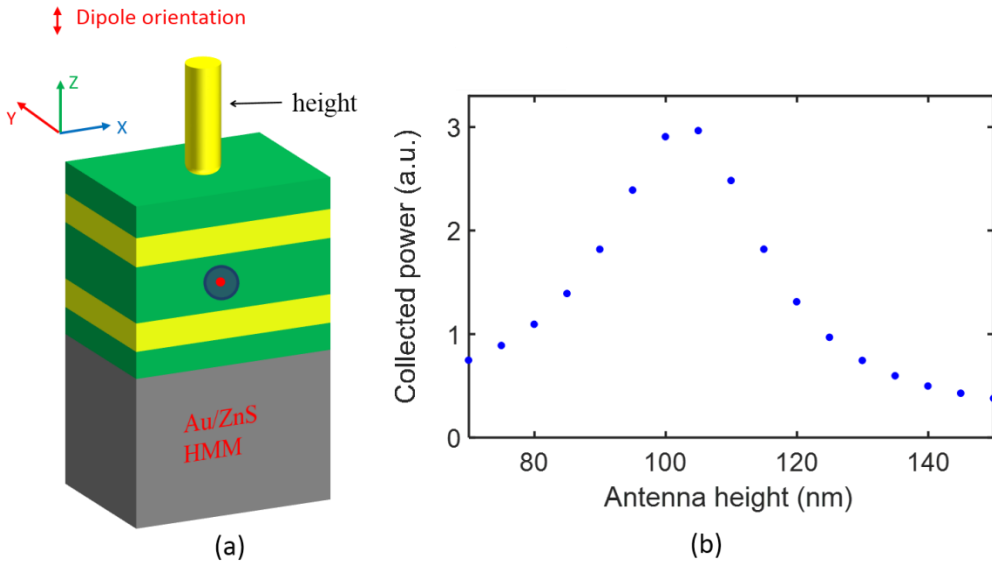


Figure 8. (a) Schematic of the single photon cylindrical antenna with variable height. (b) The collected power with varying antenna height for emission wavelength of 900 nm.

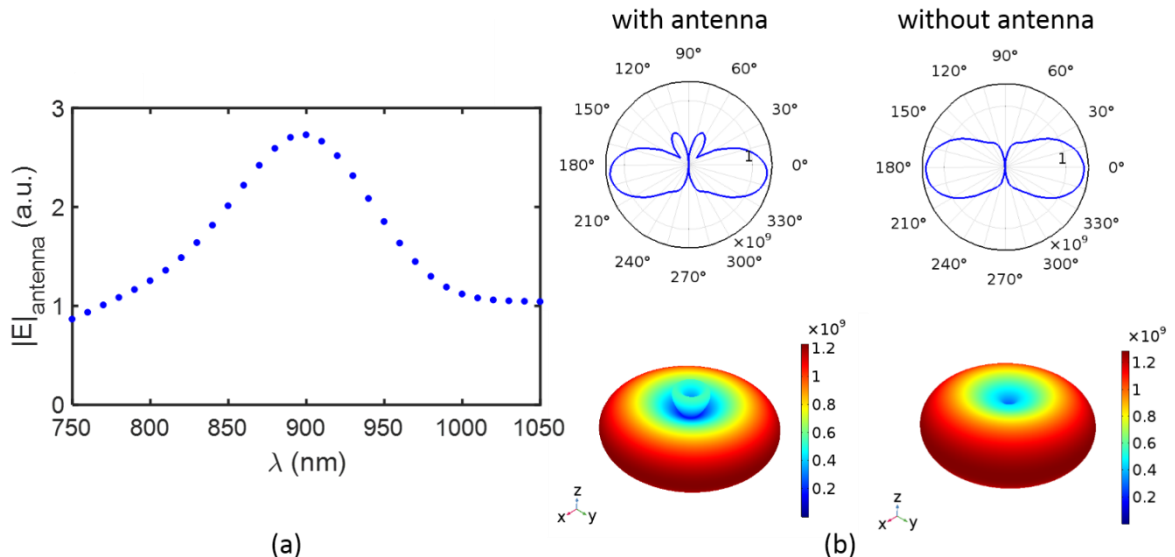


Figure 9. (a) Electric field norm on the Au antenna surface when excited by a plane wave with polarization along the z (vertical) direction and propagation vector along the x (horizontal) direction. The antenna height is 105 nm. (b) The 3D far-field norm of the electric field for dipole emission at 900 nm along with the corresponding polar plots for the case of dipole emission with and without Au antenna on the HMM structure.

Figure 9a shows the electric field norm on the antenna surface (antenna height is 105 nm) when excited by a plane wave propagating through the structure with wave-vector along the x (horizontal) direction and field polarization along the z (vertical) direction. It is clear from the above figure that the cylindrical Au antenna of height about 105 nm has a resonance mode around 900 nm. Figure 9b displays the far-field coupling of the dipole emission at 900 nm with and without the Au antenna on the HMM surface.

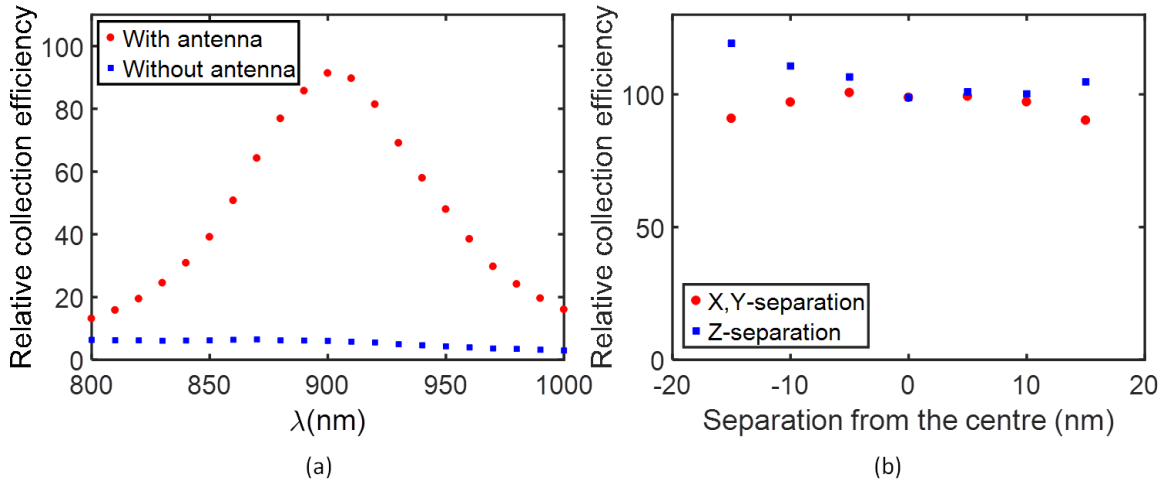


Figure 10. (a) The relative collected power as a function of wavelength with and without antenna. The antenna height was fixed at its optimum value of 105 nm. (b). The relative collected power for dipole separations from the central position along the three coordinate axis.

With the optimum antenna height of 105 nm, we calculated the total collected power for our HMM structure. The power collected using the antenna with the optimum height shows significantly large enhancement by a factor of about 100 (Figure 10 (a)). The percentage of the total net collected power with the antenna improving to about 2.2 % from 0.13 % without antenna.

Figure 10 (b) shows the variation in the collected power with dipole displacement along the three orthogonal coordinate axes for the case of dipole emitting at 900 nm. Along the z -direction, as the dipole separation from the centre increases the dipole gets closer to the metal layers leading to enhanced plasmonic resonance and enhanced antenna effect. Along the x and y directions which are both parallel to the metal-dielectric interface, the dipole experiences the same electromagnetic environment leading to negligible modifications in the collected power. Our collection scheme is therefore not critical to the dipole location below the antenna and gives the same order of enhancement for the varying dipole positions also. Though we report a substantial improvement in the net collected power by using a simple

cylindrical and patch antenna on top of the HMM structure, still a large amount of power is getting lost in the HMM structure.

To optimize the net collected power from the HMM structure, we put a cubical nanoscale patch antenna made of silver on top of the HMM structure [33, 38]. When the dipole lies close to a corner of the Ag cube we saw an increase in the total net collected power to about 6% (Figure 11). By optimizing the thickness of the HMM layers and the Ag cube we saw an increase in the total net collected power to about 15% with collection efficiency of about 50% for a collection objective with higher numerical aperture (NA) of 0.95 (Figure 12). The quantum efficiency for the dipole emission in the HMM structure was about 30%.

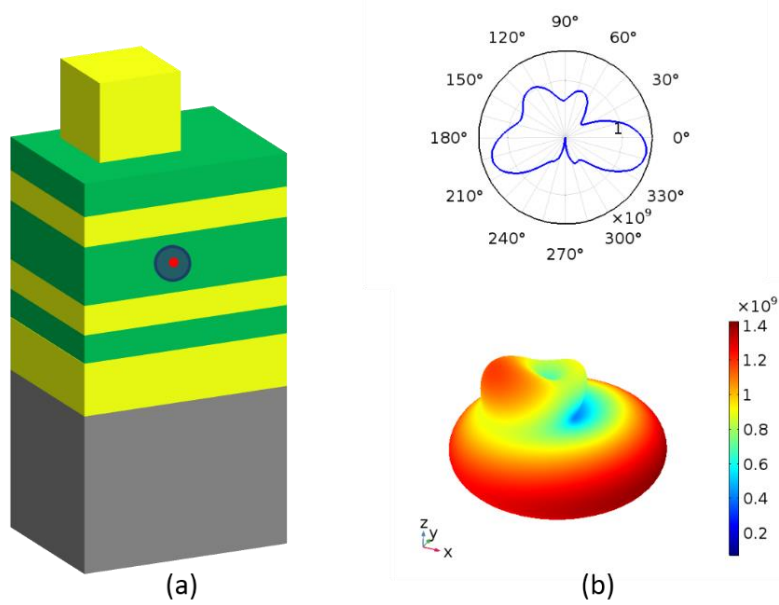


Figure 11. (a) Schematic of the cubic patch geometry on top of the HMM structure. The dipole is located near the corner of the Ag cube of size 80 nm. (b) The 3D far-field norm of the electric field for dipole emission at 900 nm along with the corresponding polar plots.

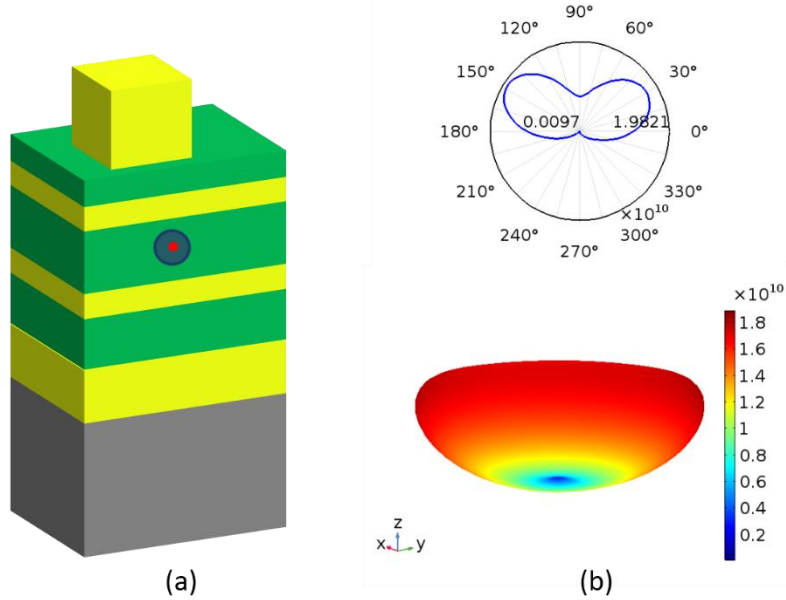


Figure 12. (a) Schematic of the cubic patch geometry on top of the modified HMM structure. The dipole is located near the corner of the Ag cube of size 110 nm. (b) The 3D far-field norm of the electric field for dipole emission at 900 nm along with the corresponding polar plots.

4. Methods:

All electromagnetic calculations of the dipole emission rate and collected power are performed using the commercial finite-element method (FEM) based COMSOL Multiphysics RF module package 5.2. The single vacancy color center is modelled as an oscillating point dipole located within the SiC nanoparticle of size 40 nm [39].

4.1. Purcell factor/emission rate calculations:

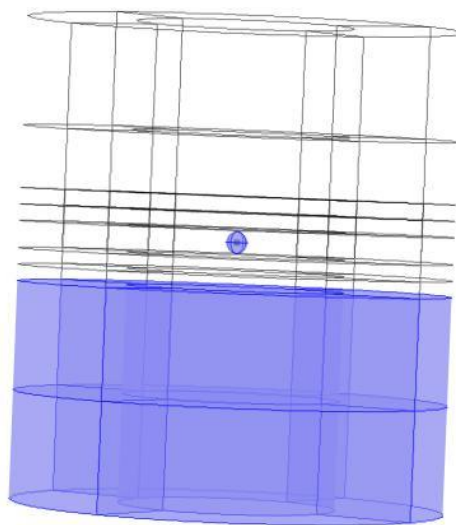


Figure 13. Computational geometry of our HMM structure. The highlighted bottom domains corresponds to the coverglass surface on which our HMM structure is place. The inner sphere corresponds to the SiC nanoparticle enclosing the point dipole.

Spontaneous emission is a purely quantum process. However since the influence of the environment is expressed through the classical LDOS, the emission rate relative to a reference system can be found by classical electromagnetic calculations also^[39]. Here in this study we are accounting for only the radiative emission process considering our emitters to have high quantum efficiency. Treating the quantum emitter as a classical point dipole, the electromagnetic fields are excited by a point current source driven at frequency $\nu = c/\lambda$. The total power radiated by the dipole is calculated over the surface of the SiC sphere as highlighted in Figure 13. The radiative spontaneous emission rate enhancement is then calculated as $R = P/P_r$, where P_r is the power corresponding to the reference system. For Purcell factor calculations the reference system is a SiC nanoparticle in vacuum. Within the whole computational domain the minimum mesh size used is 0.5 nm and the maximum mesh size used is 45 nm. Within the SiC sphere where the radiated power is calculated the minimum mesh size is kept at 0.5 nm with the maximum mesh size being 2 nm.

4.2. Collected power calculations:

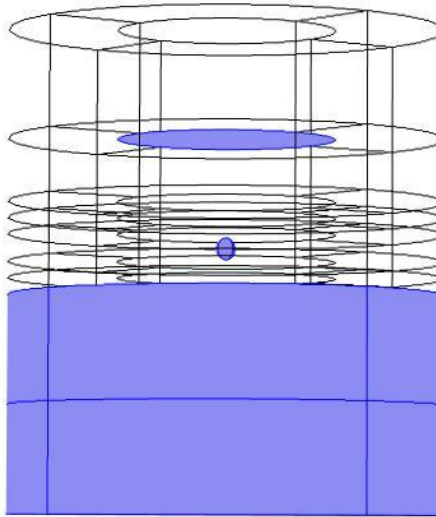


Figure 14. Computational geometry of our HMM structure with the radiated power being collected on the top highlighted surface.

Figure 14 shows the computational geometry of our HMM structure with the radiated power being collected on the top highlighted surface. The diameter of the top surface is chosen such that it acts as a collection lens with a numerical aperture of 0.6. The collected efficiency/power enhancement is then calculated as $C = P_c/P_{cr}$, where P_{cr} is the collected power corresponding to the reference system which is the case of SiC nanoparticles placed on a coverglass surface.

5. Conclusions:

We have demonstrated a simple HMM structure based on a high refractive index dielectric, ZnS, and Au layers which shows a large broadband Purcell enhancement for dipole emission in both visible and near infra-red regions. The HMM resonator is composed of gold and ZnS layers to achieve a Purcell enhancement of 400 at 850 nm and 300 at 680 nm. As the refractive indices of ZnS (2.30), SiC (2.59) and diamond (2.39) are matched, our HMM scheme is universal for all SiC and diamond based emitters. It will lead to similar enhancements for the case of SiC nanocrystals fabricated as in^[27, 40] and embedded in the ZnS middle layer; or for nanodiamond embedded in the ZnS middle layer.

Additionally, this model is particularly interesting as it can be applied to enhance emission of single photon sources not only in nanoparticles emitters but also in thin layer. This design can be extended to the case of emitters embedded in diamond^[41] or SiC thin-films by replacing the middle ZnS layer.

By replacing the dielectric with SiC itself and the metamaterial with TiN (which has similar plasmonic properties of gold) a fully CMOS compatible HMM resonator can be realised. Due to TiN being refractory material, its fabrication is compatible with thin film SiC pulsed laser deposition^[32] or SiC chemical vapor deposition, where surface color centres with dipole aligned to the main crystallographic axis can be created^[42] in addition to the above mentioned color centres.

6. Acknowledgement

FAI would like to thank Venu Gopal Achanta, TIFR, India, for useful discussions during the course of this study. FAI acknowledge University Grant Commission, India for funding through the Faculty Start-up grant.

7. References:

- [1] A. Sipahigil, R. E. Evans, D. D. Sukachev, M. J. Burek, J. Borregaard, M. K. Bhaskar, C. T. Nguyen, J. L. Pacheco, H. A. Atikian, C. Meuwly, R. M. Camacho, F. Jelezko, E. Bielejec, H. Park, M. Lončar, M. D. Lukin, *Science*, 354, 847 (2016).
- [2] P. Lodahl, S. Mahmoodian, S. Stobbe, *Reviews of Modern Physics*, 87, 347 (2015).
- [3] A. Lohrmann, B. C. Johnson, J. C. McCallum, S. Castelletto, *Reports on Progress in Physics*, 80, 034502 (2017).
- [4] T. T. Tran, K. Bray, M. J. Ford, M. Toth, I. Aharonovich, *Nat Nano*, 11, 37 (2016).

[5] F. J. Heremans, C. G. Yale, D. D. Awschalom, Proceedings of the IEEE 2016, 104, 2009; M. Widmann, S.-Y. Lee, T. Rendler, N. T. Son, H. Fedder, S. Paik, L.-P. Yang, N. Zhao, S. Yang, I. Booker, A. Denisenko, M. Jamali, S. A. Momenzadeh, I. Gerhardt, T. Ohshima, A. Gali, E. Janzén, J. Wrachtrup, Nat Mater, 14, 164 (2015).

[6] F. Fuchs, B. Stender, M. Trupke, D. Simin, J. Pflaum, V. Dyakonov, G. V. Astakhov, Nature Communications, 6, 7578 (2015).

[7] I. Aharonovich, S. Castelletto, D. A. Simpson, C. H. Su, A. D. Greentree, S. Prawer, Reports on Progress in Physics, 74, 076501 (2011).

[8] A. J. Morfa, B. C. Gibson, M. Karg, T. J. Karle, A. D. Greentree, P. Mulvaney, S. Tomljenovic-Hanic, Nano Letters, 12, 949 (2012).

[9] A. M. Berhane, K.-Y. Jeong, Z. Bodrog, S. Fiedler, T. Schröder, N. V. Triviño, T. Palacios, A. Gali, M. Toth, D. Englund, I. Aharonovich, Advanced Materials, 29, 1605092 (2017).

[10] S. Castelletto, B. C. Johnson, V. Ivády, N. Stavrias, T. Umeda, A. Gali, T. Ohshima, Nat Mater, 13, 151 (2014).

[11] A. Lohrmann, N. Iwamoto, Z. Bodrog, S. Castelletto, T. Ohshima, T. J. Karle, A. Gali, S. Prawer, J. C. McCallum, B. C. Johnson, Nature Communications, 6, 7783 (2015).

[12] H. Seo, A. L. Falk, P. V. Klimov, K. C. Miao, G. Galli, D. D. Awschalom, Nature Communications, 7, 12935 (2016).

[13] M. H. Weng, D. T. Clark, S. N. Wright, D. L. Gordon, M. A. Duncan, S. J. Kirkham, M. I. Idris, H. K. Chan, R. A. R. Young, E. P. Ramsay, N. G. Wright, A. B. Horsfall, Semiconductor Science and Technology, 32, 054003 (2017).

[14] H. Yinggang, W. Xiudong, L. Hewei, J. Hongrui, Journal of Micromechanics and Microengineering, 27, 065005 (2017).

[15] E. E. Sophia, D. Pratibha, Nanotechnology, 27, 504001 (2016).

[16] H. Kraus, V. A. Soltamov, F. Fuchs, D. Simin, A. Sperlich, P. G. Baranov, G. V. Astakhov, V. Dyakonov, Scientific Reports, 4, 5303.

[17] M. Pfender, N. Aslam, G. Waldherr, P. Neumann, J. Wrachtrup, Proceedings of the National Academy of Sciences 2014, 111, 14669 (2014).

[18] M. Pelton, Nat Photon, 9, 427 (2015).

[19] A. F. Koenderink, ACS Photonics, 4, 710 (2017).

[20] K. J. Russell, T.-L. Liu, S. Cui, E. L. Hu, Nat Photon, 6, 459 (2012).

[21] S. Schietinger, M. Barth, T. Aichele, O. Benson, Nano Letters, 9, 1694 (2009).

[22] A. Poddubny, I. Iorsh, P. Belov, Y. Kivshar, Nat Photon, 7, 948 (2013).

[23] W. D. Newman, C. L. Cortes, Z. Jacob, J. Opt. Soc. Am. B, 30, 766 (2013).

[24] T. Galfsky, H. N. S. Krishnamoorthy, W. Newman, E. E. Narimanov, Z. Jacob, V. M. Menon, *Optica*, 2, 62 (2015).

[25] M. Y. Shalaginov, S. Ishii, J. Liu, J. Liu, J. Irudayaraj, A. Lagutchev, A. V. Kildishev, V. M. Shalaev, *Applied Physics Letters*, 102, 173114 (2013).

[26] M. Y. Shalaginov, V. V. Vorobyov, J. Liu, M. Ferrera, A. V. Akimov, A. Lagutchev, A. N. Smolyaninov, V. V. Klimov, J. Irudayaraj, A. V. Kildishev, A. Boltasseva, V. M. Shalaev, *Laser & Photonics Reviews*, 9, 120 (2015).

[27] S. Castelletto, A. F. M. Almutairi, G. Thalassinos, A. Lohrmann, R. Buivid, D. W. M. Lau, P. Reineck, S. Juodkazis, T. Ohshima, B. C. Gibson, B. C. Johnson, *Opt. Lett.*, 42, 1297 (2017).

[28] D. H. Hwang, J. H. Ahn, K. N. Hui, K. S. Hui, Y. G. Son, *Nanoscale Research Letters*, 7, 26 (2012).

[29] S. Castelletto, J. P. Harrison, L. Marseglia, A. C. Stanley-Clarke, B. C. Gibson, B. A. Fairchild, J. P. Hadden, Y. L. D. Ho, M. P. Hiscocks, K. Ganesan, S. T. Huntington, F. Ladouceur, A. D. Greentree, S. Prawer, J. L. O. Brien, J. G. Rarity, *New Journal of Physics*, 13, 025020 (2011).

[30] L. Li, E. H. Chen, J. Zheng, S. L. Mouradian, F. Dolde, T. Schröder, S. Karaveli, M. L. Markham, D. J. Twitchen, D. Englund, *Nano Letters*, 15, 1493 (2015).

[31] M. A. Capano, S. D. Walck, P. T. Murray, D. Dempsey, J. T. Grant, *Applied Physics Letters*, 64, 3413 (1994).

[32] F. A. Inam, R. Kumar, N. Rameshwari, D. Lau, S. Ghosh, B. C. Gibson, S. A. Ramakrishna, S. Castelletto, "Studying Quantum Light Emission from Color Centers Embedded in Ultra-thin-Films SiC from Pulsed Laser Deposition", presented at *13th International Conference on Fiber Optics and Photonics*, Kanpur, 2016/12/04 (2016).

[33] G. M. Akselrod, C. Argyropoulos, T. B. Hoang, C. Ciraci, C. Fang, J. Huang, D. R. Smith, M. H. Mikkelsen, *Nature Photonics*, 8, 835 (2014).

[34] R. J. Glauber, M. Lewenstein, *Physical Review A*, 43, 467 (1991).

[35] H. Yuan, X. Jiang, F. Huang, X. Sun, *Scientific Reports*, 6, 30818 (2016).

[36] E. Hecht, *Optics*, Addison-Wesley (2002).

[37] L. Novotny, *Physical Review Letters*, 98, 266802 (2007).

[38] T. B. Hoang, G. M. Akselrod, M. H. Mikkelsen, *Nano Letters*, 16, 270 (2016).

[39] Y. Xu, J. S. Vučković, R. K. Lee, O. J. Painter, A. Scherer, A. Yariv, *J. Opt. Soc. Am. B*, 16, 465 (1999).

[40] A. Muzha, F. Fuchs, N. V. Tarakina, D. Simin, M. Trupke, V. A. Soltamov, E. N. Mokhov, P. G. Baranov, V. Dyakonov, A. Krueger, G. V. Astakhov, *Applied Physics Letters*, 105, 243112 (2014).

[41] S. Stehlik, M. Varga, P. Stenclova, L. Ondic, M. Ledinsky, J. Pangrac, O. Vanek, J. Lipov, A. Kromka, B. Rezek, *ACS Applied Materials & Interfaces*, 9, 38842 (2017).

[42] A. Lohrmann, S. Castelletto, J. R. Klein, T. Ohshima, M. Bosi, M. Negri, D. W. M. Lau, B. C. Gibson, S. Prawer, J. C. McCallum, B. C. Johnson, *Applied Physics Letters*, 108, 021107 (2016).